





Modelling and mapping burn severity of prescribed and wildfires across the southeastern United States (2000-2022)

Melanie K. Vanderhoof^{A,*}, Casey E. Menick^A, Joshua J. Picotte^B, Kevin M. Robertson^C, Holly K. Nowell^C, Chris Matechik^C and Todd J. Hawbaker^A

For full list of author affiliations and declarations see end of paper

*Correspondence to:

Melanie K. Vanderhoof US Geological Survey, Geosciences and Environmental Change Science Center, Denver Federal Center, MS980, Denver, CO 80225, USA

Email: mvanderhoof@usgs.gov

Received: 16 August 2024 **Accepted:** 7 December 2024 **Published:** 10 January 2025

Cite this: Vanderhoof MK et al. (2025) Modelling and mapping burn severity of prescribed and wildfires across the southeastern United States (2000–2022). International Journal of Wildland Fire 34, WF24137. doi:10.1071/WF24137

© 2025 The Author(s) (or their employer(s)). Published by CSIRO Publishing on behalf of IAWF.

This is an open access article distributed under the Creative Commons Attribution 4.0 International License (CC BY).

OPEN ACCESS

ABSTRACT

Background. The southeastern United States ('Southeast') experiences high levels of fire activity, but the preponderance of small and prescribed fires means that existing burn severity products are incomplete across the region. Aims. We developed and applied a burn severity model across the Southeast to enhance our understanding of regional burn severity patterns. Methods. We used Composite Burn Index (CBI) plot data from across the conterminous US (CONUS) to train a gradient-boosted decision tree model. The model was optimised for the Southeast and applied to the annual Landsat Burned Area product for 2000–2022 across the region. Key results. The burn severity model had a root mean square error (RMSE) of 0.48 ($R^2 = 0.70$) and 0.50 ($R^2 = 0.37$) for the CONUS and Southeast, respectively. The Southeast, relative to CONUS, had lower mean absolute residuals in low and moderate burn severity categories. Burn severity was consistently lower in areas affected by prescribed burns relative to wildfires. Conclusions. Although regional performance was limited by a lack of high burn severity CBI plots, the burn severity dataset demonstrated patterns consistent with low-severity, frequent fire regimes characteristic of Southeastern ecosystems. Implications. More complete data on burn severity will enhance regional management of fire-dependent ecosystems and improve estimates of fuels and fire emissions.

Keywords: burn severity, burned area, Composite Burn Index, CBI, differenced Normalized Burn Ratio, dNBR, Landsat, longleaf pine, Monitoring Trends in Burn Severity, MTBS, post-fire, prescribed fire, Southeast US, wildfire, wildland fire.

Introduction

Wildland fires, both prescribed burns and wildfires, alter ecosystem conditions and processes (Bowman et al. 2009; Franklin et al. 2016), with the amount of change reflected by burn severity (Meng and Zhao 2017). Satellite imagery has been widely used to develop operational burned area products (Randerson et al. 2017; van der Werf et al. 2017; Humber et al. 2018; Hawbaker et al. 2020a) and to monitor burn severity (Meng and Zhao 2017; Miller et al. 2023). Within the United States, the southeastern US ('Southeast') experiences the largest number of wildland fire ignitions (Randerson et al. 2017; Short 2022), the greatest occurrence of wildfire in the wildland-urban interface (WUI) (Thomas and Butry 2014; Radeloff et al. 2023) and the most active application of prescribed fire (Nowell et al. 2018; Kolden 2019; Melvin 2020). However, the great majority of fires are small, and most are prescribed, making them challenging to detect remotely owing to their limited extent and relatively low severity. Therefore, efforts to track regional burned areas and burn severity are underdeveloped (Picotte et al. 2020; Hawbaker et al. 2020a; Teske et al. 2021). Improving regional characterisation of burn severity, quantified as the degree of loss of aboveground and soil organic matter and the corresponding change in spectral reflectance (Keeley 2009), is important to improve estimates of emissions (Larkin et al. 2014), fuel loads (Boisramé et al. 2022), wildfire risk

(Kolden 2019) and impacts to natural resources (Weiss *et al.* 2019), as well as to inform invasive plant management (Alba *et al.* 2015).

Southeastern forests, savannas and grasslands have a long history of fire, with Indigenous people maintaining a frequent fire regime prior to colonisation (Fowler and Konopik 2007; Ryan et al. 2013). European settlers burned to encourage grasses for cattle grazing, and since the 1800s, to manage for northern bobwhite 'quail' (Colinus virginanus) (Johnson and Hale 2002). In more recent decades, burning on both public and private lands is also applied to benefit timber production, reduce hazardous fuel loads, restore ecosystems and enhance wildlife habitat (Addington et al. 2015; Kobziar et al. 2015; Mason and Lashley 2021). The smaller size of Southeast fires, relative to the western US, is typically attributed to constraints on the application of prescribed fire and landscape fragmentation into smaller parcels (Kobziar et al. 2015), which limits the spread of accidental and lightningignited fires (Johnson and Hale 2002). As burn severity generally increases with time since fire and associated fuel accumulation (Godwin and Kobziar 2011; Malone et al. 2011), land managers aim to apply prescribed fire intervals that are as short as feasible to preclude higher-severity wildfires (Johnson and Hale 2002; Kobziar et al. 2015). Remotely tracking burned area and severity from these small, lowintensity fires is challenging, exacerbated by high annual precipitation and frequent summer afternoon thunderstorms that result in regular cloud cover, reducing the frequency of clear images (Picotte and Robertson 2011a; Vanderhoof et al. 2021). Additionally, most of the fire-dependent communities in the region are characterised by rapid rates of regrowth from perennial vegetation that survives fire, shortening image selection windows and making accurate field data collection difficult (Godwin and Kobziar 2011; Malone et al. 2011).

The remote characterisation of burn severity has commonly relied on the Normalized Burn Ratio (NBR) spectral index or the differenced NBR (dNBR) index mapped from pre- and post-fire NBR images (Picotte et al. 2021; Miller et al. 2023). Although widely used, dNBR depends in part on the amount and type of pre-fire vegetation (Zhu et al. 2006). Consequently, other burn severity indices, including the relative dNBR (RdNBR; Miller et al. 2009) and the relativised burn ratio (RBR; Parks et al. 2014), have emerged to help control for the effects of pre-fire vegetation. These are particularly helpful in unforested areas where NBR can respond more to soil wetness than plant coverage (Malone et al. 2011; Salvia et al. 2012). A lack of consensus for a preferred spectral index (Whitman et al. 2020; Howe et al. 2022; Saberi and Harvey 2023) has resulted in burn severity products often providing multiple indices or reporting a categorical severity value. Burn severity is most comprehensively mapped by (1) the MOSEV global burn severity database and a global Landsat forest burn severity (He et al. 2024), both of which attribute burn severity for the Moderate Resolution Imaging Spectroradiometer (MODIS)

burned area product (MCD64A1; Alonso-González and Fernández-García 2021), (2) the Monitoring Trends in Burn Severity (MTBS) product (Eidenshink *et al.* 2007), which maps fires >400 hectares in the western US and >200 hectares in the eastern US from Landsat products (Picotte *et al.* 2020), and (3) Burned Area Emergency Response (BAER) and Rapid Assessment of Vegetation Condition (RAVG) assessments, which both map burn severity on federal forestlands (Hudak *et al.* 2007). Collectively, these efforts produce consistent burn severity maps for large wildfires across the US and most fires on federal land. However, they do not map burn severity for small wildfires, most prescribed fires and many fires on private lands, complicating efforts to track complete patterns of burned area and severity over time.

Ecological interpretation of remotely sensed burn severity estimates commonly relies on Composite Burn Index (CBI) field plots (Key and Benson 2006). CBI assesses damage to substrates and above-ground biomass using a continuous index with values ranging from 0.0 (unburned) to 3.0 (high severity). The statistical relationships between CBI and NBR or dNBR tend to reflect post-fire vegetation condition more than soil condition (Hudak et al. 2007). CBI plots have been effectively related to dNBR across the western and conterminous US (CONUS) using correlation (He et al. 2024), multiple regression approaches including polynomial regression models (Zhu et al. 2006), sigmoidal regression models (Lutz et al. 2011; Picotte et al. 2021) and non-linear least squares regression models (Howe et al. 2022), as well as multi-variable random forest models (Parks et al. 2019). Even so, obtaining adequate accuracy across the Southeast remains challenging. For example, although the model of Parks et al. (2019) showed a strong explanatory power across CONUS, the accuracy for Florida, where most of the model's Southeast training points were located, was poor. Studies focusing on selected, common natural community types in Florida and Georgia have successfully related CBI with NBR and dNBR (e.g. Godwin and Kobziar 2011; Picotte and Robertson 2011b); however, they have not been validated for broader geographic application.

Improving our characterisation of burn severity across the Southeast will provide data useful to monitor silviculture and ecosystem condition and support prescribed fire and ecosystem restoration (Larkin et al. 2014; Weiss et al. 2019; Jaffe et al. 2020). Here, we built on localised efforts within the Southeast (e.g. Godwin and Kobziar 2011; Malone et al. 2011; Picotte and Robertson 2011b) to improve our capacity to map burn severity at landscape scales across the region. We used CBI plot data compiled across CONUS (Picotte et al. 2019) to develop a machine learning model that includes spectral indices from multiple windows to map burn severity. The model was applied to all burned areas across the Southeast (2000–2022) mapped by the US Geological Survey's Landsat Burned Area (BA) product, which identifies burned area > 2 ha, regardless of fire

type (wildfire or prescribed) or land ownership (Hawbaker *et al.* 2020*a*). Focusing on forested areas identified as burned by the BA product, we sought to characterise patterns and trends in burn severity across the region. Our research questions included:

- Can we improve on efforts to map burn severity in the Southeast?
- 2. How do vegetation and forest type influence burn severity?
- 3. Are there annual trends in average burn severity over the study period?
- 4. Is burn severity influenced by fire history (i.e. recent fire frequency) and fire type (i.e. prescribed or wildfire)?

Methods

Study area

Our study area extends across most of the Southeast, including the entirety of Florida, Georgia, South Carolina, North Carolina, Alabama, Mississippi, Louisiana, and parts of Texas, Kentucky, Tennessee, Arkansas and Virginia (Fig. 1). The

extent was defined by the Southeast FireMap project (Tall Timbers 2024), which in turn was based on the historical distribution of longleaf pine (Pinus palustris), a native pine species that is highly dependent on fire and the focus of conservation and restoration efforts across its extent (Barnett 1999). Much of this region is part of the Southeast Plains and Coastal Plains ecoregions (Omernik and Griffith 2014), notable as global biodiversity hotspots (Noss et al. 2015) and a significant producer of forest products (Howard and Liang 2019). Land cover is dominated by forests (34%), woody wetlands (14%), agriculture (22%) and developed areas (10%) (Homer et al. 2020). Forested systems most commonly include pine plantations, unmanaged closedcanopy broadleaf forests in uplands or wetlands, and opencanopy forests, woodlands and savannas. On the modern landscape, dominant tree species include loblolly pine (P. taeda L.), shortleaf pine (P. echinata Mill.), longleaf pine, slash pine (P. elliottii Engelm.), and many species of oak (Quercus spp.) and other broadleaf deciduous tree species (Ruefenacht et al. 2008). Annual precipitation across the region averages 1324 mm, while annually the maximum and minimum temperature averages 24.4 and 12.0°C, respectively (1990-2020; Abatzoglou 2013).

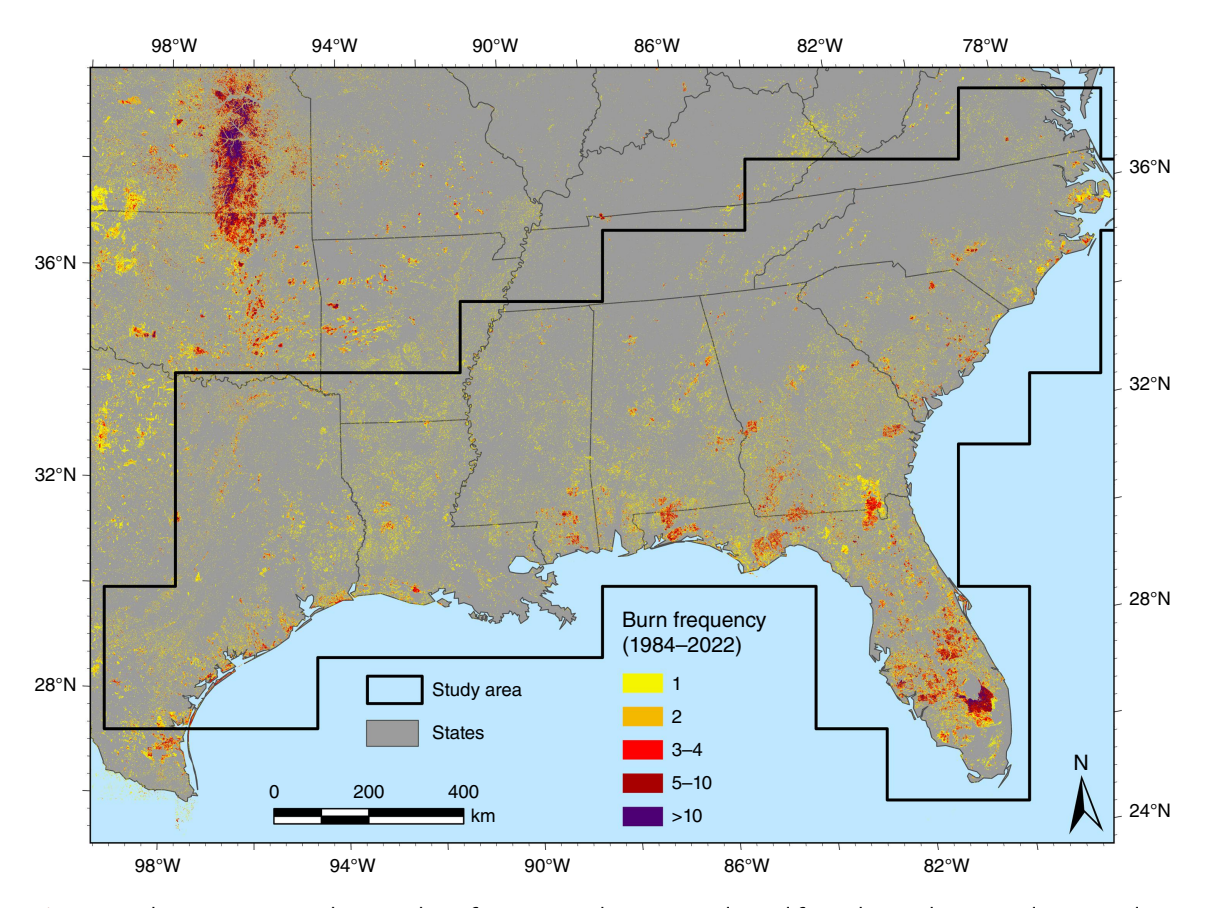


Fig. 1. Study area extent in relation to burn frequency or burn count, derived from the Landsat Burned Area product at an annual time step (1984–2022). Longer time range provided to reflect long-term geographic differences in burn frequency.

CBI training data

We used CBI plot data collected across the CONUS for model training and validation, while targeting performance improvements in the Southeast. Utilising the CONUS-wide burned CBI plots, relative to the Southeast alone, provided training data across more geographically diverse fire events, represented greater variability in burn severity and added more high burn severity training data for use in our Southeast-focused application. The CBI data included 5532 plots from multiple independent projects or field campaigns following 232 fire events occurring between 1996 and 2018 compiled by Picotte et al. (2019). These data were supplemented with an additional 276 CBI plots from 23 fires collected in 2017 and 2018 across Arizona and New Mexico (Reiner et al. 2022), for a total of 5808 forested burned CBI plots, including 904 prescribed and wildfire burned CBI plots across the Southeast (Fig. 2a). A total of 438 (7.5%) CBI plots were removed during data checks if they did not have a recorded fire date (n = 26), had notably erroneous plot locations (n = 15), or occurred in grasslands or agriculture fields as determined using high-resolution aerial imagery (n = 264). We also excluded plots if field measurement occurred more than 1 year post-fire in subtropical regions, defined here as Florida, owing to rapid revegetation obscuring post-fire effects (n = 133) (Key and Benson 2006). Unburned CBI plot data were excluded as well because sampling was inconsistent across the datasets. Instead, a stratified sampling approach was employed to generate 552 unburned (i.e. CBI = 0) pseudo-plots proportional to approximately 10% of the CBI plots collected for each individual fire event. We generated randomly distributed pseudo-plots within 500 m-1 km of collected field plots, excluding areas mapped as burned by the Landsat BA product. To control for spectral outlier values, pseudoabsence plots with dNBR values below the 2.5th and above the 97.5th percentile were also removed. CBI plots were excluded from model development if insufficient imagery, as described in the 'Landsat image selection and preprocessing' section, was available to generate all spectral predictor layers. These exclusions left 5038 burned field plots and 495 unburned pseudo-plots (total = 5533) across CONUS that were used in model development (Fig. 2). Within the Southeast, plots included 598 burned field plots and 57 unburned pseudo-plots, representing 11.8% of the CBI plots. CBI median \pm s.d. was 1.64 \pm 0.77 across CONUS compared with 1.49 ± 0.53 across the Southeast, and while 991 plots across CONUS had a CBI of > 2.5, only 34 occurred within the Southeast.

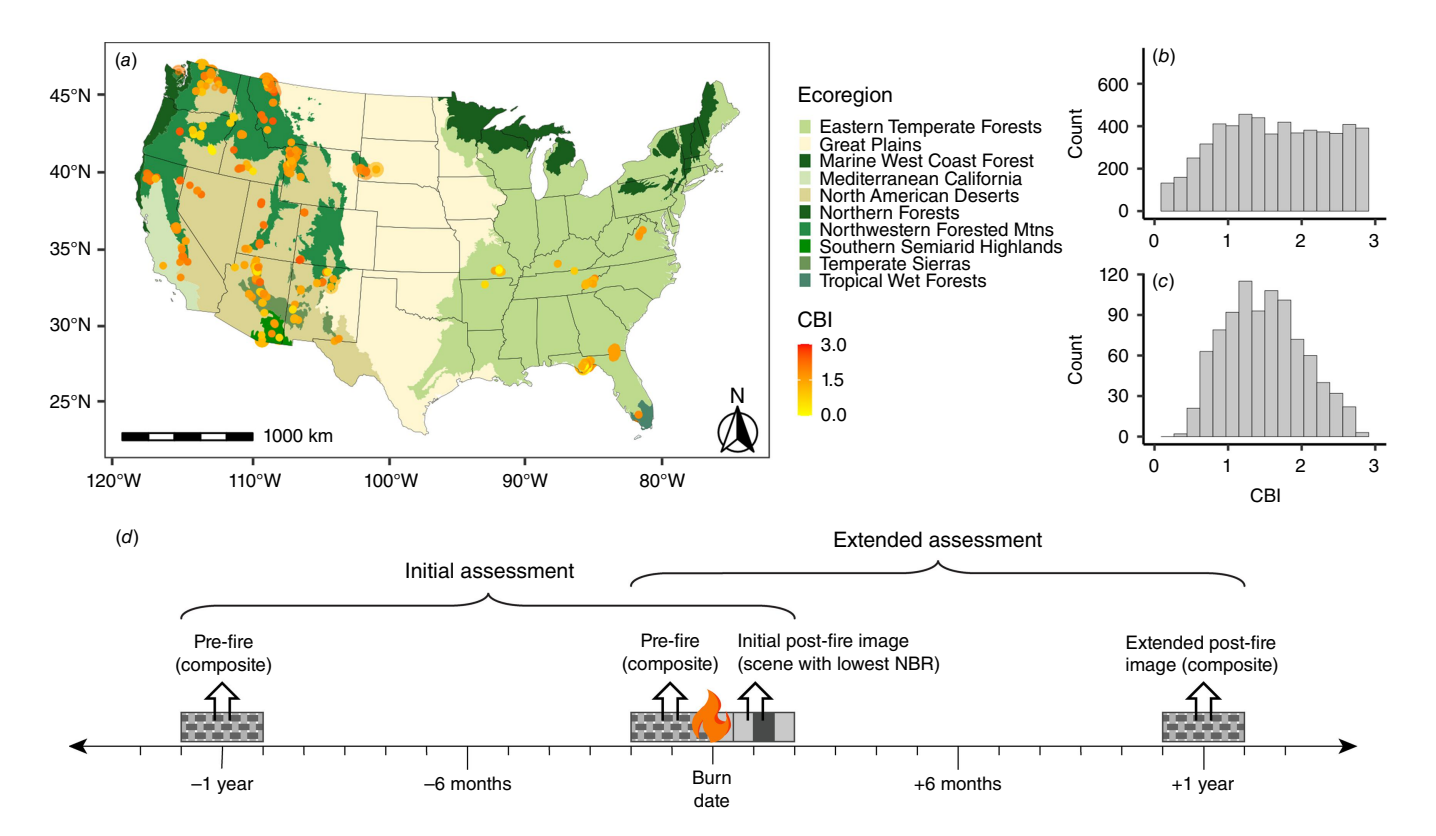


Fig. 2. (a) Locations of Composite Burn Index (CBI) field plots used to develop the burn severity model; (b) histograms of plot counts by CBI value for CBI values >0 across the conterminous US; and (c) within the Southeast study area; and (d) pre-fire and post-fire image selection approach where, for each spectral variable, the (1) initial assessment, (2) extended assessment, (3) initial post-fire image, and (4) extended post-fire image values were considered as potential model variables. NBR, Normalized Burn Ratio.

Landsat image selection and pre-processing

We attributed the CBI plot data using Landsat Surface Reflectance 5-8 Collection 2 imagery. Cloud, cloud shadow, open water and snow pixels were masked using the Function of Mask (FMask; Zhu and Woodcock 2014). To determine suitable model predictors, we considered the spectral bands: red, NIR (near infrared), SWIR1 (shortwave infrared) and SWIR2, as well as spectral indices that have previously been shown to be helpful in evaluating fire effects and post-fire vegetation conditions (Table 1). For each spectral index and band, we calculated (1) initial post-fire assessment from preand post-fire imagery, (2) extended post-fire assessment from pre- and post-fire imagery, (3) initial post-fire image, and (4) extended post-fire image values (Fig. 2d). Initial assessments evaluated same-season post-fire imagery to reflect immediate, first-order fire impacts, whereas extended assessments evaluated imagery the following year to account for delayed mortality and survivorship (Key and Benson 2006). We calculated initial assessments with a post-fire Landsat scene that was uniquely selected for each burned pixel by identifying the date of lowest NBR (i.e. highest severity) in the 2-month period following fire detection. Previous research in the region has determined that burn severity assessment should be conducted within 2 months following a fire to account for rapid post-fire regrowth of top-killed vegetation that can obscure spectral signatures and reduce model performance (Picotte and Robertson 2011a). Extended assessments were measured using a post-fire composite image, generated from the median pixel value 1-year post-fire (Busby et al. 2023). Pre-fire images were generated from 2-month median image composites 1 year pre-fire for initial assessments and immediately preceding the fire event for extended assessments (Fig. 2d). Although minimal differences have been found between using paired images (one pre- and postfire image) versus image composites, compositing, or averaging across multiple images, can be more easily automated (Whitman et al. 2020; Saberi and Harvey 2023). When differencing pre- and post-fire imagery, an offset value differencing the imagery within unburned vegetation can help account for phenological differences between pre- and post-fire image dates (Miller and Thode 2007; Miller et al. 2009). After testing the application of automated offset values representing a range of unburned buffers from 100 m to a Landsat Analysis Ready Data (ARD) tile, we found that applying offset values showed no improvement in model performance, similarly to Picotte and Robertson (2011b), and they were therefore not used in model development or application.

Long-term climate patterns help determine fire regimes, in part owing to their influence on vegetation type and condition (Liu and Wimberly 2015). Therefore, we also considered the normal (1990–2019) annual (1) precipitation (PR), (2) potential evapotranspiration (PET), and (3) aridity

index (AI; PET/PR) derived from TerraClimate (~4 km; Abatzoglou *et al.* 2018) as potential covariates in the model. As fuel loads are seasonally dependent, fire seasonality was also considered where the fire day of year (DOY), as reported in the CBI metadata, was binned into winter (DOY 335–59), spring (DOY 60–151), summer (DOY 152–243) and fall (DOY 244–334). A complete list of the variables considered is shown in Table 1.

Model development

CBI plots of burn severity were modelled as a function of Landsat-derived variables, including spectral indices calculated from post-fire, initial and extended assessment windows, as well as long-term climate variables. We used the eXtreme Gradient Boosting model, XGBoost (Chen and Guestrin 2016), a machine learning algorithm that uses a gradient boosting decision tree framework with regularisation processes to avoid overfitting and improve generalisability. During model fitting, we evaluated 432 unique hyperparameter combinations (selected hyperparameters are shown in bold), including number of trees [300, 500, 700], maximum tree depth [0, 3, 5], minimum child weight [3, 5, 7, 10], learning rate [0.01, 0.05, 0.10, 0.30], gamma [0.0, 0.2, 0.4], and subsampled data splits [0.8]. Including highly correlated covariates in decision tree models can bias model predictions and deflate variable importance, making models difficult to interpret (Murphy et al. 2010; Dormann et al. 2013). Therefore, we used a stepwise forward selection routine to concurrently identify the optimal set of hyperparameters and predictors (Sherrouse and Hawbaker 2023). For each hyperparameter combination, predictors were sequentially tested and selected for inclusion based on which predictors minimised model root mean square error (RMSE). During each step, remaining predictors were removed if they were highly correlated (R > 0.70) with any of the selected predictors. This process was repeated until the improvement in the model's RMSE was < 1.0% with any additional variables. The iterative predictor selection process was performed using grouped five-fold cross validation across all model hyperparameter combinations to identify the best-performing model that minimised RMSE. To evaluate model performance (e.g. R^2 and mean square error (MSE)), we used grouped k-fold cross-validation (e.g. Gallagher et al. 2020). The entire dataset was divided into five folds and grouped by fire event to avoid training and testing on the same fire. The model was trained on all folds except one and evaluated on the remaining fold in each iteration. Model performance was averaged across the five iterations. Variable permutation importance was calculated by permuting features 100 times to evaluate model variable importance for both CONUS and the Southeast. Permutation importance provides a more robust assessment of each variable's contribution to model predictions by evaluating performance on a test set, while randomly shuffling individual

 Table 1.
 Spectral and environmental variables considered for inclusion as model predictors.

Predictor type	Time frame	Name	Abbreviation	Definition	Reference
Landsat Bands	Initial assessment	Red	Red	Landsat TM/ETM + Band 3, OLI Band 4	-
	Extended assessment	Near infrared	NIR	Landsat TM/ETM + Band 4, OLI Band 5	-
	Initial post-fire image	Shortwave infrared 1	SWIR1	Landsat TM/ETM + Band 5, OLI Band 6	-
	Extended post-fire image	Shortwave infrared 2	SWIR2	Landsat TM/ETM + Band 7, OLI Band 7	-
Spectral indices	Initial assessment	Normalized Burn Ratio	NBR	NIR – SWIR2/NIR + SWIR2	García and Caselles (1991), Key and Benson (2006)
	Extended assessment	Normalized Burn Ratio 2	NBR2	SWIR1 – SWIR2/SWIR1 + SWIR2	García and Caselles (1991), Key and Benson (2006)
	Initial post-fire image	Normalized Burn Ratio Thermal	NBRT	(NIR - (SWIR2 \times Thermal))/(NIR + (SWIR2 \times Thermal))	Holden <i>et al.</i> (2005)
	Extended post-fire image	Normalized Difference Vegetation Index	NDVI	NIR – Red/NIR + Red	Tucker (1979)
		Normalized Differenced Moisture Index	NDMI	NIR – SWIRI/NIR + SWIRI	Gao (1996)
		Enhanced Vegetation Index	EVI	$2.5 \times (NIR - Red)/(NIR + (6.0 \times Red) - (7.5 \times Blue) + 1.0)$	Huete et al. (2002)
		Soil Adjusted Vegetation Index	SAVI	$1.5 \times (NIR-Red)/(NIR + Red + 0.5)$	Huete (1988)
		Burned Area Index	BAI	$1/((0.1 - Red)^2 + (0.06 - NIR)^2)$	Chuvieco et al. (2002)
		Char Soil Index	CSI	NIR/SWIR2	Smith et al. (2007)
		Global Environmental Monitoring Index	GEMI	$\eta \times (1.0-0.25 \times \eta)$ - ((Red - 0.125)/(1 - Red)); $\eta = (2 \times (NIR^2 - Red^2) + (1.5 \times NIR) + (0.5 \times Red))/(NIR + Red + 0.5)$	Pinty and Verstraete (1992)
		Mid InfraRed Burn Index	MIRBI	(10.0 × SWIR2) - (9.8 × SWIR1) + 2.0	Trigg and Flasse (2001)
		NIR-red ratio	VI43	NIR/Red	Tucker (1979)
		NIR-SWIR1 ratio	VI45	NIR/SWIR1	Epting et al. (2005)
		SWIR1-SWIR2 ratio	VI57	SWIRI/SWIR2	Epting et al. (2005)
Climate	30-year (1990–2019) Normalized annual mean	Potential evapotranspiration	PET	-	Abatzoglou et al. (2018)
		Precipitation	PR	-	Abatzoglou et al. (2018)
		Aridity index	Al	PET/PR	Abatzoglou et al. (2018)
Season	Season of fire event	Fire season	Fire season	Burn date in day of year 335–359 (winter), 60–151 (spring), 152–243 (summer), 244–334 (fall (autumn))	-

TM, Thematic Mapper; ETM+, Enhanced Thematic Mapper Plus; OLI, Operational Land Imager.

features to better reflect model generalisability and predictive power. Variables that show a greater decrease in accuracy score on exclusion indicate higher importance to model prediction.

CBI model application to the Landsat BA product

The gradient boosted decision tree model was applied to pixels that were already identified as burned using the Landsat BA product (30-m resolution; 1984-present; Hawbaker et al. 2020a, 2020b), which operationally maps burned area extent for Landsat Collection 2 imagery across CONUS with <80% cloud cover. Both wildfires and prescribed fires > 2 ha are mapped, but fire type is not distinguished. Validated with commercial, high-resolution imagery, the Landsat BA product showed an omission (i.e. false negative) and commission (i.e. false positive) error of 19 and 41% for CONUS, and 45 and 37% for the eastern US, respectively (Hawbaker et al. 2020a). Although the Landsat BA product maps more burned area in the Southeast compared with other burned area products such as MTBS or MODIS MCD64A1 (Hawbaker et al. 2020a), we acknowledge that the product still under-maps low-severity prescribed fire (Teske et al. 2021; Vanderhoof et al. 2021). Sources of error intrinsic to the image collection, such as poor or uneven atmospheric conditions, residual clouds or cloud shadows, or surface reflectance conversion errors, can introduce higher-than-expected rates of commission error in a minority of images. Consequently, all classified images were visually reviewed and problematic images were removed (1.4% of classified images) prior to creating annual composites from the time series (Hawbaker et al. 2020b).

We applied the burn severity model to the annual suite of Landsat BA products (2000-2022) across 76 Landsat ARD tiles (\sim 150 \times 150 km each). The fire date was defined using the annual burn date raster, which represents the day of year (1-366) of the first Landsat scene in which a burned area was observed. Consequently, if a pixel burned more than once in a year, burn severity would be calculated for the first fire event only. The percentage of burned pixels that lacked one or more clear-sky observations representing either pre- or post-fire conditions was substantially greater prior to 2000; therefore, the burn severity model was applied to the annual Landsat BA products for 2000-2022. Each unique burn date was used to identify corresponding 2-month windows for the 1-year pre- and post-fire dates and immediate pre- and post-fire dates (Fig. 2d). The pixel burn date was also applied to attribute fire seasonality, using the burn date DOY as defined in the 'Landsat image selection and pre-processing' section. The generated predictor stack for each unique burn date was used to predict CBI values from the trained model. CBI values were not predicted for pixels that lacked predictor imagery (average of 7.3% of burned area annually, ranging from 3% in 2004 to 24% in 2013) owing to extensive cloud cover or other image quality

constraints. Pixels predicted to have a CBI < 0 were a minority case (< 0.0001% of pixels) and were reclassified as CBI = 0.001.

Burn severity patterns

To evaluate spatial and temporal patterns in burn severity, we randomly generated 50,000 points per year (2000–2022) across our mapped burn severity. The points were limited to non-grassland and non-agriculture Southeast burned area (n = 1,150,000), and herein are referred to as the sampled predicted CBI points. Fire activity within grassland and agricultural areas was assumed to either result in the nearcomplete combustion of vegetation or represent a highly managed land use and was therefore excluded from the analysis. Agriculture and grassland extent was defined as herbaceous, pasture/hay and cultivated crop cover type, as mapped by the National Land Cover Database (NLCD; Homer et al. 2020) using the nearest NLCD year (2001, 2006, 2011, 2016, 2019, 2021). Sampled predicted CBI points were selected to be a minimum of 200 m from one another to minimise the influence of spatial autocorrelation in the analysis of burn severity.

Patterns in burn severity were summarised by forest type (Ruefenacht *et al.* 2008), land cover using nearest year NLCD (Homer *et al.* 2020) and public–private land ownership (PAD-US 3.0; US Geological Survey (USGS) 2022). Forest types that represented >2% of the burned area were reported. As the MTBS dataset (Eidenshink *et al.* 2007) is the most comparable burn severity dataset, MTBS burn severity was visually compared with the model-predicted burn severity. Burn severity within MTBS is categorical and low severity is assigned as the default value in herbaceous vegetation types (Picotte *et al.* 2020). Therefore, comparisons with MTBS were restricted to burned areas dominated by forest, shrub, or woody wetland vegetation types as defined by NLCD.

We limited our evaluation of temporal trends in burn severity to forested land cover, where most fires in the region occur, defined using the nearest year NLCD. We used the non-parametric Mann-Kendall test for significant temporal trends. Trends in forest burn severity were separated into months in which prescribed fire dominates (December-April; Cummins et al. 2023) and months in which wildfire dominates (May-November; Slocum et al. 2007; Donovan et al. 2023), recognising the co-occurrence of both fire types within a given month is common. Additionally, as burn severity is influenced by meteorological conditions (Parks and Abatzoglou 2020), we correlated the sampled predicted CBI points to annual average Palmer Drought Severity Index (PDSI). As the Mann-Kendall test is most commonly utilised for trend analysis, we applied the non-parametric Spearman Rank-Order Correlation. Monthly PDSI was derived from TerraClimate (4 km), where increasing positive values represent wetter conditions and

decreasing negative values represent drier conditions (Abatzoglou *et al.* 2018).

Differences in burn severity attributable to fire type (prescribed fire versus wildfire) were further explored by compiling burn polygons attributed with burn type across the Southeast. Sources of attributed burned area included the (1) LANDFIRE Public Events Geodatabase (LANDFIRE 2022), (2) the Southeastern US Prescribed Fire Permit Database (Cummins et al. 2023), and (3) the Fire Program Analysis fire-occurrence database (FPA FOD) (Short 2022). Attributed burned area was required to be colocated with an area mapped as burned by the Landsat BA product in the same year while occurring within a forested NLCD land cover type. The FPA FOD and southeastern US Prescribed Fire Permit Database are points datasets. These points were limited to those with a burn type attributed as wildfire (e.g. incendiary, arson, or wildfire) or prescribed burn (e.g. broadcast burn, prescribed burn, or hazardous fuel reduction). Points were excluded for alternative burn types, including burn piles. Points with over 25 records for the same coordinates were also excluded as this suggested that, even after accounting for the possibility of consecutive day permit requests, a non-specific location (e.g. a county centroid) was likely reported. Remaining points were converted to an attributed polygon extent, reflecting the corresponding polygon record from the Landsat BA product, and compiled with the LANDFIRE attributed polygons.

We limited the sampled predicted CBI points (n=1,150,000) to those overlapping the forested burned area attributed as prescribed (n=183,831) or wildfire (n=88,826) (Supplementary Fig. S1). To test the influence of fire type on burn severity, differences in CBI burn severity between prescribed and wildfire were evaluated by forest type (Ruefenacht *et al.* 2008). To test the expectation that more frequent fires may reduce burn severity (Hunter and Robles 2020), we categorised burn frequency or burn count (2000–2022) as (1) 1 fire, (2) 2–3 fires, and (3) 4+ fires (Vanderhoof *et al.* 2022). Significant differences in CBI values were determined using the non-parametric Welch Satterthwaite *t*-test.

Results

Model performance

The selected model had an RMSE of 0.48, an MSE of 0.23 and an R^2 of 0.70 for CBI predictions across CONUS. Model performance was similar but slightly weaker within the Southeast alone, with an RMSE of 0.50 and MSE of 0.26; however, the explanatory power was weaker relative to CONUS, with an R^2 of 0.37 (Table 2, Fig. 3). Despite the lower explanatory power, when residuals were compared by burn severity category, the Southeast had a lower mean absolute residual for observed low (residuals = 0.31)

Table 2. Composite Burn Index (CBI) model performance (shaded grey) relative to previously published national CBI modelling efforts.

Geographic extent	R ²	RMSE	Source
CONUS	0.70	0.48	Modelled results
CONUS	0.58	0.58	Picotte et al. (2021)
CONUS	0.72	0.47	Parks et al. (2019)
Southeast	0.37	0.50	Modelled results
Southeast	0.18	0.69	Picotte et al. 2021
Florida	0.01	0.53	Parks et al. (2019)
North Carolina	<0.01	0.57	Parks et al. (2019)

The Southeast results were calculated from the CBI observations within our study area. Results for states located entirely within the study area are presented for Parks *et al.* (2019). CONUS, conterminous United States.

compared with 0.38, respectively) and moderate (residuals = 0.34 compared with 0.37, respectively) burn severity relative to the non-Southeast (Table 3). For the non-Southeast, in contrast, high burn severity showed the lowest absolute residuals of any severity class, 0.32, and much lower absolute residuals than high-severity plots in the Southeast (residuals = 0.84) (Table 3). In comparing residual values in the growing season relative to the dormant season, the non-Southeast had a lower mean absolute residual in the growing season relative to the Southeast, but within the Southeast, the dormant season, relative to the growing season had a lower mean absolute residual, suggesting that burn severity predictions in the Southeast were not impacted by dormant season conditions (Table 3).

The lower explanatory power in the Southeast was partly a consequence of a smaller range of variability in CBI compared with CONUS (Fig. 2c). Outside the Southeast, CBI ≥ 2.5 and CBI ≥ 2.7 comprised 18 and 11% of the CBI plots, respectively. In comparison, within the Southeast, CBI ≥ 2.5 and CBI ≥ 2.7 comprised 3 and 0.5% of the CBI plots, respectively. R^2 values are influenced by the range of variability in the response variable. To demonstrate this effect, we randomly sampled non-Southeast CBI plots ≥ 2.7 at a 25% sampling rate (n=134) to artificially increase the proportion of high-severity plots, as defined in Table 3, to 50% of the region's moderate-burn severity plot count. Including these high-severity non-Southeast plots, the explanatory power increased from $R^2=0.37$ to $R^2=0.62$.

The selected predictors included two extended assessment variables, dNBR and dSWIR1 (differenced shortwave infrared 1), two initial assessment variables, dBAI (differenced Burned Area Index) and dNBR2, an extended post-fire image variable, vi57 (SWIR1/SWIR2 ratio), as well as the fire season, and normal annual PET and PR (Table 1, Fig. 4). Permutation importance calculations showed that all variables had a significant (P < 0.01) influence on model performance, with a positive decrease in accuracy scores for all calculated iterations. For CONUS, the dNBR extended

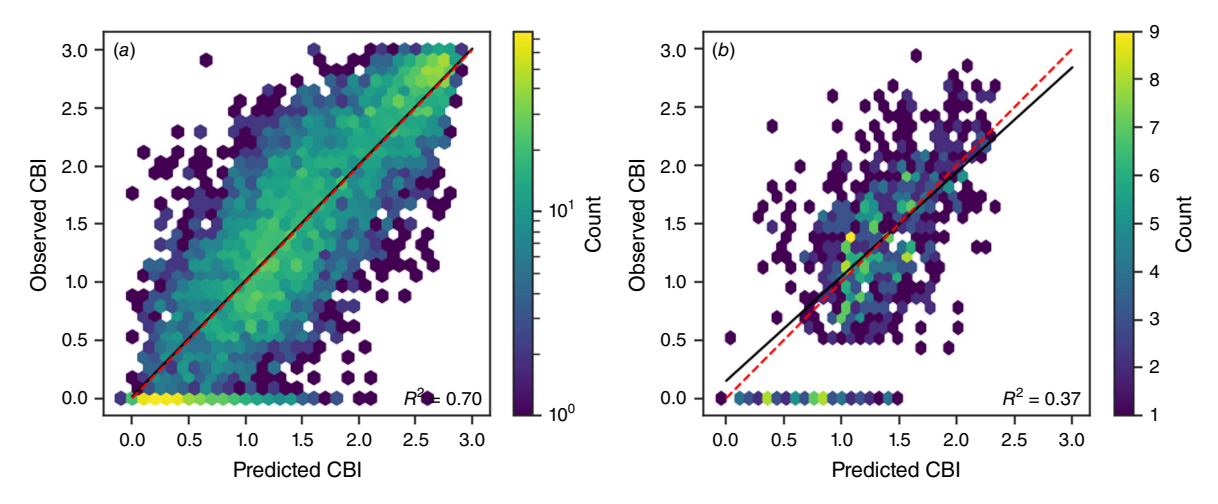


Fig. 3. Comparison of field-observed CBI (Composite Burn Index) values with model-predicted CBI values for (a) all continental US plots, and (b) southeastern US plots. Point density is depicted by hexagonal bins, with colours indicating the concentration of points per bin. Dashed red line represents the 1:1 identity line, solid black line represents the line of linear regression between the observed and predicted values.

Table 3. Differences in mean absolute residuals across the Southeast compared with outside of the Southeast by burn severity class derived from the observed Composite Burn Index (CBI) (low: ≤1.25, moderate: >1.25 and ≤2.25) and season (dormant: 15 November–28 February, growing: 1 March–14 November). s.d., standard deviation.

Burn severity class	Region	Mean absolute residual (s.d.)	Count
Unburned	Southeast	0.67 (0.355)	57
Unburned	Non- Southeast	0.48 (0.403)	438
Low	Southeast	0.31 (0.235)	228
Low	Non- Southeast	0.38 (0.285)	1543
Moderate	Southeast	0.34 (0.267)	336
Moderate	Non- Southeast	0.37 (0.294)	1577
High	Southeast	0.84 (0.395)	34
High	Non- Southeast	0.32 (0.287)	1320

Season	Region	Mean absolute residual (s.d.)	Count
Dormant	Southeast	0.34 (0.261)	155
Dormant	Non-Southeast	0.51 (0.375)	75
Growing	Southeast	0.40 (0.321)	500
Growing	Non-Southeast	0.37 (0.302)	4803

assessment showed the greatest variable permutation importance, followed by the vi57 extended post-fire image (Fig. 4), reflecting the influence of delayed mortality in western forest fires. In contrast, the Southeast model depended most strongly on the dNBR extended assessment

and the dBAI and dNBR2 initial assessments, indicating a greater regional importance of initial assessment variables (Fig. 4). Although climate and fire season variables were selected for inclusion, they showed lower variable importance, such that the coarser native spatial resolution of these variables was not visually evident in the mapped burn severity. An example of how the CBI plots translated to MTBS and modelled CBI burn severity is shown in Supplementary Fig. S2.

Spatial patterns of burn severity

The Landsat BA product mapped a total of 171,350 km² of burned area (median of 7147 km² burned per year) across the Southeast from 2000 to 2022. Although CBI burn severity was variable within individual fires, low to moderate burn severity dominated across the region (Fig. 5). Burn severity was mapped for many wildfires and prescribed fires that were too small to be mapped by other programs such as MTBS or MOSEV. Examples of differences between the Landsat BA product and MTBS in mapped burned area extent and corresponding burn severity are shown in Fig. 6, which shows prescribed burns within Fort Stewart's Back Gate (Fig. 6a), the Apalachicola National Forest (Fig. 6b) and tree plantations on private land (Fig. 6c). Fig. 7 represents our general observation that where a fire is mapped by both datasets, the CBI burn severity and MTBS appear to be detecting similar underlying patterns in burn severity, in part reflecting overlap in the indices used.

Average burn severity was greatest in emergent herbaceous wetlands (CBI = 1.39) and woody wetlands (CBI = 1.31), and lowest in deciduous forest (CBI = 1.00) (Table 4). Within forest types, average burn severity was highest in bald cypress and water tupelo forests (CBI = 1.38). Within pine forest types, slash pine showed

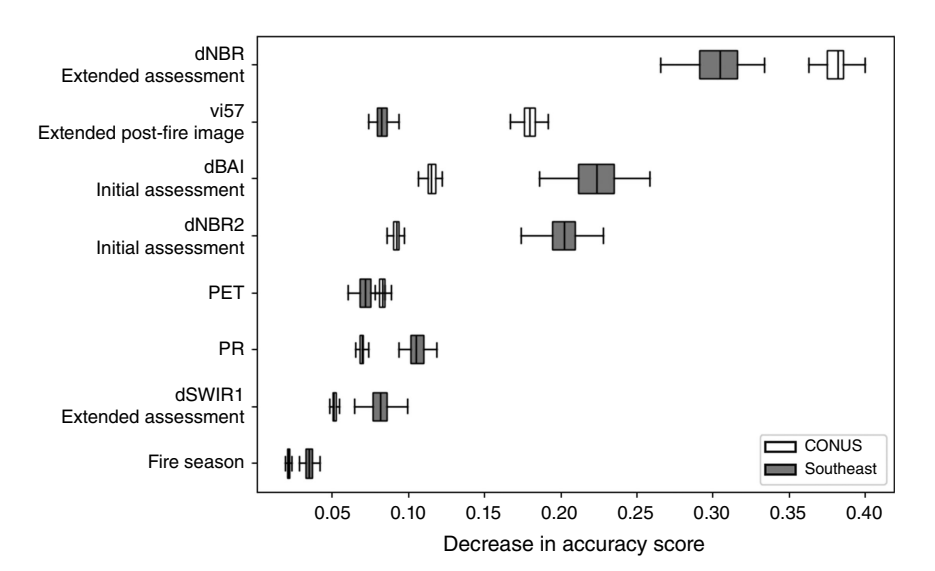


Fig. 4. Variable permutation importance for the best-performing model. All variables showed a significant (*P* < 0.01) influence on model prediction, for both CONUS and the Southeastern US. Variability in the decrease in accuracy score for 100 iterations was plotted for each predictor in the full model in white, ranked in order of decreasing importance. For the southeastern US, variable permutation is plotted in grey. dNBR, differenced Normalized Burn Ratio; dSWIRI, differenced shortwave infrared 1; vi57, SWIRI/SWIR2 ratio; dBAI, differenced Burned Area Index; PET, annual mean potential evapotranspiration; PR, annual mean precipitation; CONUS, conterminous United States.

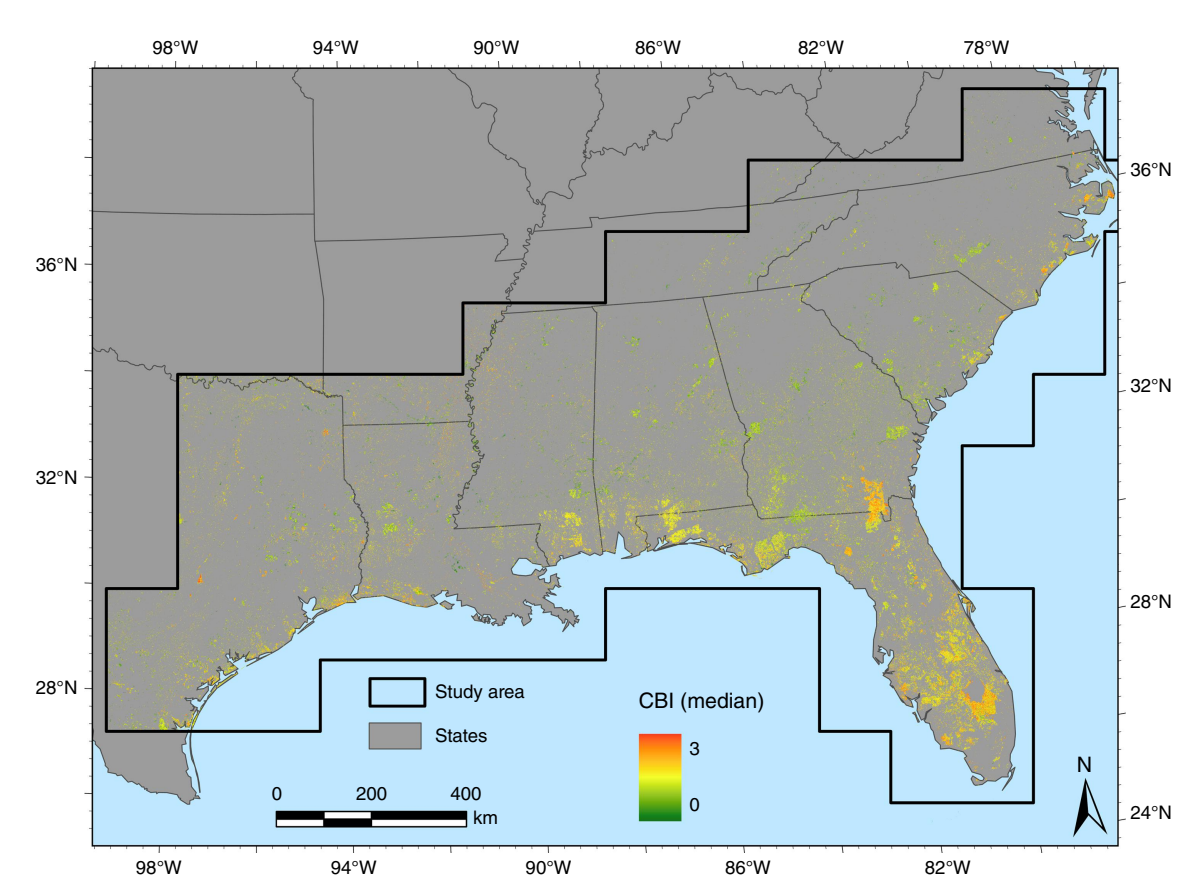


Fig. 5. Predicted Composite Burn Index (CBI) or burn severity across the study area (2000–2022). Where repeat fires occurred, the median CBI value is shown. Although our analysis excluded agricultural and grassland burned areas, burn severity for all vegetation types is shown here for informational purposes only.

the highest burn severity (CBI = 1.32), and loblolly pine the lowest (CBI = 1.11) (Table 4). Public land comprised only 10.9% of the study area but showed a higher median CBI than private burning, 1.23 relative to 1.18, respectively, and contributed 37.6% of the total area burned (Table 4).

Temporal trends in burn severity

Over the 23 years analysed for this study, we observed a significant (P < 0.001) decline in average mapped CBI burn severity (Fig. 8a). This decline was evident in months in which prescribed fire dominates (December–May) as well as

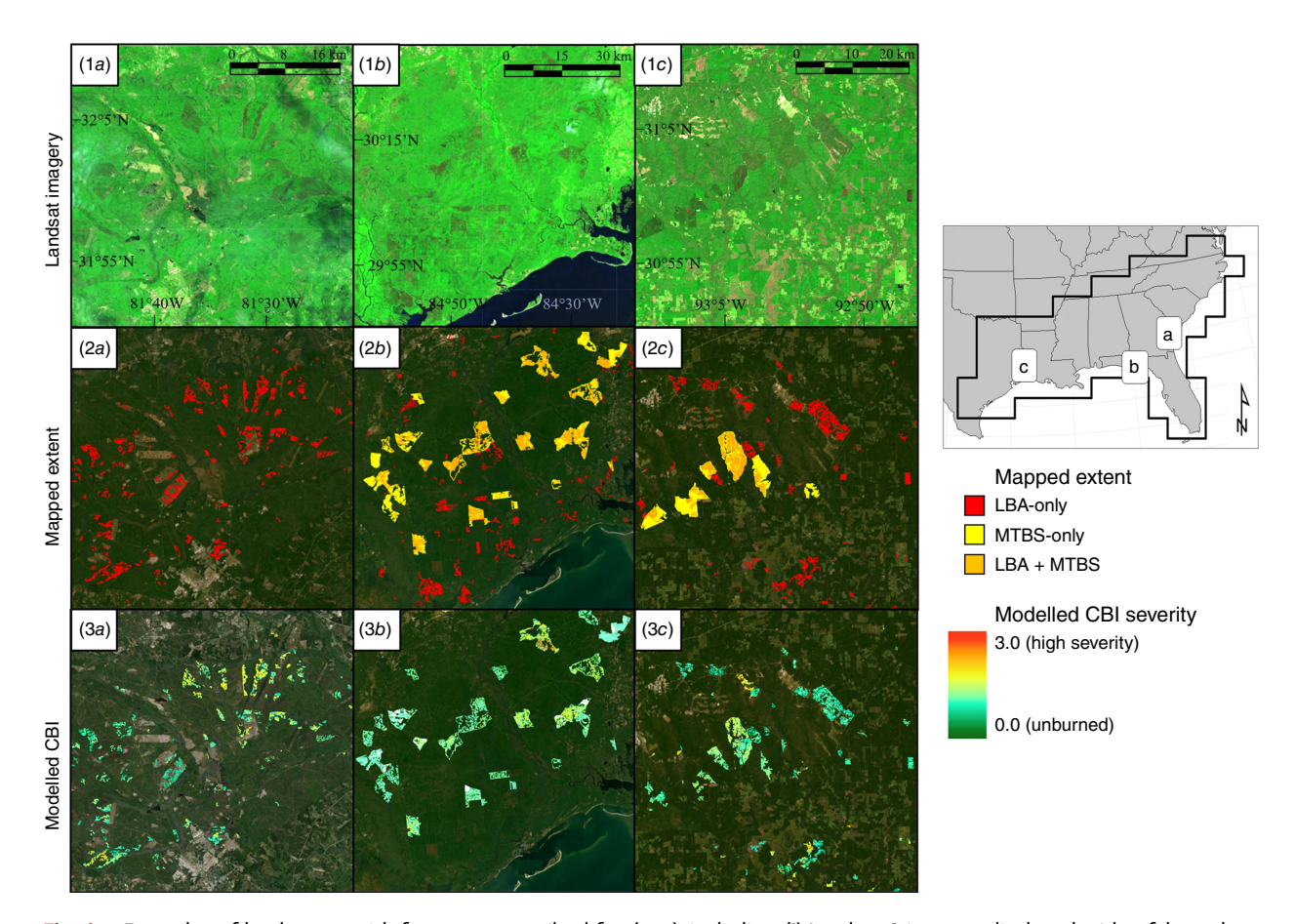


Fig. 6. Examples of landscapes with frequent prescribed fire (a–c), including: (1) Landsat-8 imagery displayed with a false colour composite (shortwave infrared 2, near-infrared, red) reflecting the peak of fire activity, collected on (a) 24 March 2021, (b) 18 April 2016, and (c) 8 February 2018); (2) the extent of the corresponding annual burned area mapped by the Landsat Burned Area (LBA) Product only (red), Monitoring Trends in Burn Severity (MTBS) only (yellow), or both products (orange) in (a) 2021, (b) 2016 and (c) 2018; and (3) corresponding modelled Composite Burn Index (CBI) burn severity for the areas mapped as burned by the Landsat Burned Area Product.

months in which wildfire dominates (June–November) (Fig. 8b). Testing for the potential influence of meteorological conditions on the temporal trends, we observed a significant negative correlation between PDSI and CBI, indicating greater average burn severity in drier years. This correlation was significant in both forest (deciduous, mixed, evergreen) and woody wetland vegetation types (Fig. 8c).

Influence of fire type on burn severity

Relative to wildfires and across forest types and fire frequencies, prescribed burns consistently showed a lower average burn severity (Supplementary Fig. S3). However, all three pine forest types showed a convergence in burn severity as fire frequency increased. For example, loblolly pine showed a substantial difference in burn severity between prescribed and wildfires (median CBI difference of 0.40–0.42) where fire frequency was lower (i.e. 1–3 burns within the 23 year period), but this difference declined to a CBI difference of 0.12 where fire frequency was high (i.e. 4+ burns)

(Supplementary Fig. S3). Similarly, in longleaf pine, the differences in severity between prescribed and wildfire diminished as fire frequency moved from a single fire to moderate fire, and then high fire regime, with the mean CBI difference decreasing from 0.16 to 0.08, and 0.02, respectively. The exception to this pattern was the bald cypress/water tupelo forested wetland type, for which severity progressively increased with greater fire frequency (Supplementary Fig. S3).

Discussion

Addressing regional challenges to mapping burn severity

In this analysis, we predicted continuous CBI burn severity values for areas in the Southeast mapped as burned by the Landsat BA product, encompassing >170,000 km² of burned area over a 23-year period. This effort produced

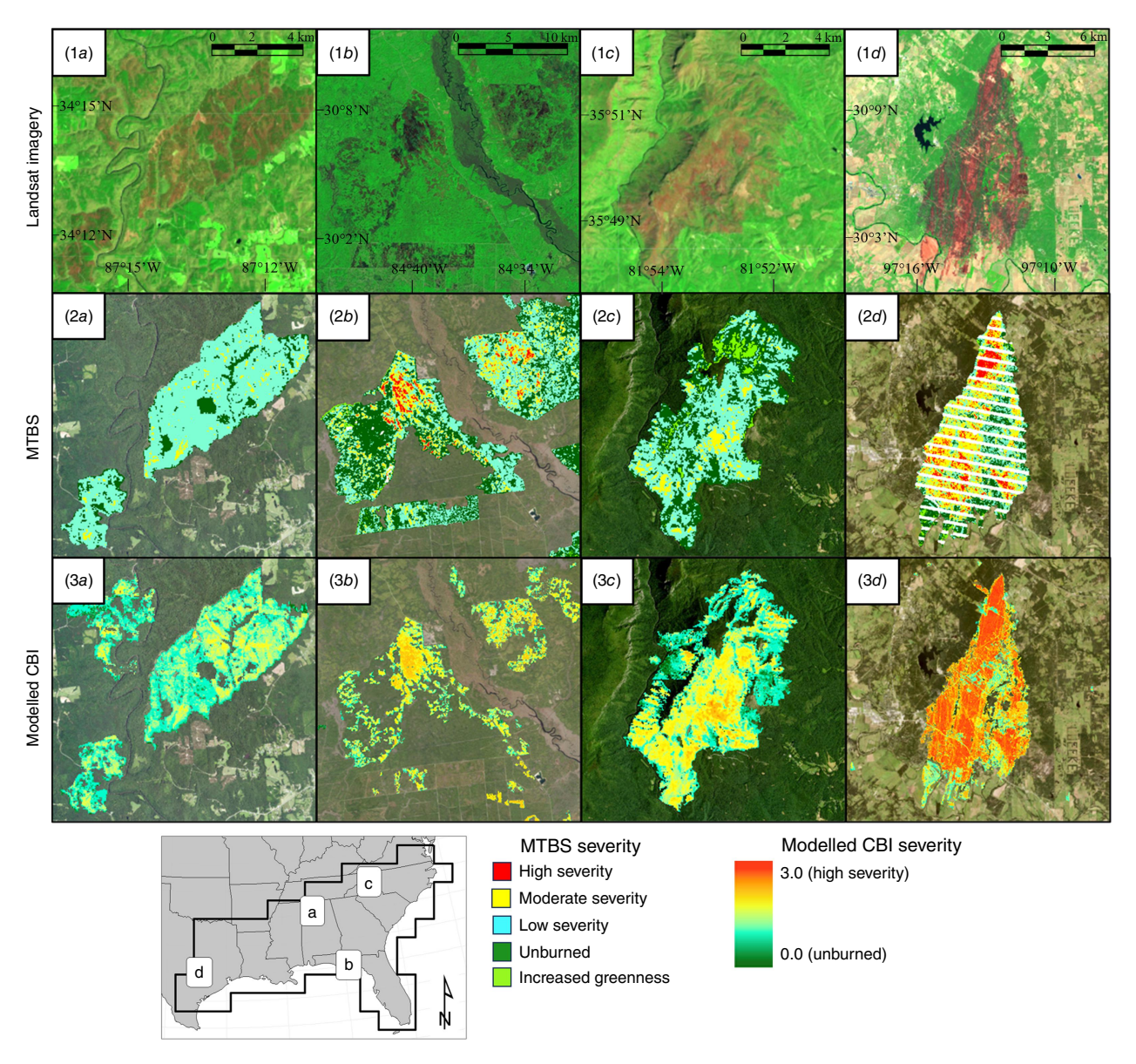


Fig. 7. Four burned areas (a-d) visible with Landsat imagery (I) using a false colour composite (shortwave infrared 2, near-infrared, red) collected by (Ia) Landsat-8 on 7 April 2016, (Ib) Landsat-5 on 24 February 2008, (Ic) Landsat-8 on 14 April 2017, and (Id) Landsat-5 on 11 September 2011. Example differences are shown in mapped burn severity between the (2) Monitoring Trends in Burn Severity (MTBS) dataset (3) and the model-predicted Composite Burn Index (CBI) burn severity.

the most inclusive post-fire burn severity data for the region to date, mostly notably contributing new burn severity data for small and prescribed fires that are the most challenging to map and characterise. Average CBI by land cover ranged from 1.00 to 1.39, suggesting that most of the burned area in the Southeast is of low burn severity, a finding consistent with prior efforts in the region (Picotte and Robertson 2011b; Picotte *et al.* 2021). While the present effort greatly expanded burn severity data, the burned area product still shows higher rates of omission across the Southeast relative to other regions (Hawbaker *et al.* 2020a) and under-maps prescribed fire in particular (Melvin 2020), suggesting that

the goal of providing complete fire datasets for the Southeast is still ongoing.

In this effort, image selection and model variables were used to help address some of the challenges inherent to a Landsat-based burn severity mapping approach in the Southeast, including frequent cloud cover, rapid post-fire revegetation and the dominance of low burn severity associated with prescribed fires (Godwin and Kobziar 2011; Picotte and Robertson 2011b; Vanderhoof *et al.* 2021). Although models developed for the western US predominantly rely on dNBR and extended assessment imagery windows (Miller *et al.* 2023), we also considered initial assessments

Table 4. Total burned area (2000–2022) and predicted Composite Burn Index (CBI) values by land cover, forest type and land ownership.

Land cover	Total area burned (km²) (relative %)	Median CBI (s.d.)
Evergreen forest	42,532 (24.8%)	1.17 (0.38)
Woody wetlands	24,953 (14.6%)	1.31 (0.46)
Shrub/scrub	12,953 (7.6%)	1.26 (0.41)
Emergent herbaceous wetlands	11,597 (6.8%)	1.39 (0.43)
Deciduous forest	7023 (4.1%)	1.00 (0.40)
Mixed forest	4584 (2.7%)	1.06 (0.44)
Landowner	Total area burned (km²) (relative%)	Median CBI (s.d.)
Public	64,409 (37.6%)	1.23 (0.41)
Private	106,906 (62.4%)	1.18 (0.44)
Forest type	Total area burned (km²) (relative %)	Median CBI (s.d.)
Loblolly pine	38,456 (22.4%)	1.11 (0.40)
Slash pine	25,237 (14.7%)	1.32 (0.40)
Longleaf pine	8895 (5.2%)	1.27 (0.30)
Loblolly pine/hardwood	4361 (2.5%)	1.08 (0.38)
Mixed upland hardwoods	4093 (2.4%)	1.13 (0.40)
Bald cypress/water tupelo	4020 (2.3%)	1.38 (0.44)
White oak/red oak/ hickory	3837 (2.2%)	1.03 (0.41)
Sweetbay/swamp tupelo/red maple	3609 (2.1%)	1.29 (0.42)
Other forest types	12,035 (7%)	1.15 (0.44)

Total area burned based on the annual Landsat Burned Area product. Of the total burned area, 39% was in land cover types not included in the analysis. Median CBI calculated from the sampled points with the standard deviation (s.d.) in parentheses. Forest types representing <2% of burned area were consolidated into the 'other forest types' class.

to capture immediate post-fire effects. Initial assessment variables of dBAI and dNBR2, for example, both showed greater variable importance in the Southeast relative to CONUS. This finding suggests that a regional model that could rely more heavily on initial assessments may be preferable if we had a greater abundance of CBI data representing diverse ecosystems and burn severities across the region. As the range of burn severity in the Southeast was more truncated (Fig. 2), we utilised the full CONUS CBI dataset, taking advantage of western forest plots that can be ecologically and structurally similar to the Southeast (Bigelow *et al.* 2017). This approach provided a broader range of fire conditions on which to train the model, but the more limited range of CBI values in the Southeast likely influenced the regional model performance metrics (Gelman and Hill 2007).

Creating unburned CBI pseudo-plots in the Southeast was also a challenge. We documented higher mean absolute residuals for unburned pseudo-plots in the Southeast compared with the non-Southeast (Table 3). This could be attributed to under-mapped prescribed fires (Melvin 2020), expansive silviculture activities (Howard and Liang 2019) and seasonal fluxes in forested wetland water level (Malone et al. 2011; Salvia et al. 2012) creating greater regional spectral variability. Expansion of CBI data collection in the Southeast, as well as considering alternatives to CBI (e.g. Miller et al. 2023) that may be more reflective of Southeast fire regimes will likely benefit future national burn severity modelling efforts.

Considering diverse spectral indices associated with vegetation conditions and post-fire effects beyond dNBR may have also improved model performance in the Southeast. Across the region, canopy cover can obscure surface fires that lack crown scorch (Key and Benson 2006), and seasonal flooding may weaken the relationship between dNBR and burn severity (Malone et al. 2011; Salvia et al. 2012). In the future, airborne or satellite lidar, for instance, could potentially improve post-fire characterisation of changes in forest structure (e.g. Huettermann et al. 2023). Model choice may also be important. Although simpler statistical models (e.g. regressions) can facilitate easier communication of a model and its results to decision makers, these approaches may have limited ability to distinguish between gradients of severity so that machine-learning or deep-learning models may be necessary to improve burn severity class separability (Hultquist et al. 2014).

Cloud cover remains a challenge. In our effort, an annual average of 7.3% of burned pixels were not assigned a burn severity value owing to cloudy images limiting data availability in one or more of the imagery windows. Further, the number of clear-sky images included in composites averaged four in the Southeast compared with seven across CONUS. However, no significant relationship between the number of images and the absolute residual value was observed. Regardless, incorporating datasets that provide a similar spatial resolution but denser time series with improved opportunities to detect and characterise burn severity prior to recovery, like Sentinel-2 or the harmonised Landsat Sentinel-2 (HLS) dataset (Vanderhoof *et al.* 2021; Howe *et al.* 2022), is worth exploring, though modelling multidecadal patterns will still depend on the Landsat archive.

Ecological and land management implications

The patterns of burn severity identified in our analysis reflect patterns of land use and natural vegetation as well as emphasise the utility of our algorithm for natural resource management. For example, prescribed fire corresponded to lower burn severity estimates than wildfire. Although this finding was expected because the application of prescribed fire is designed in part to limit burn severity

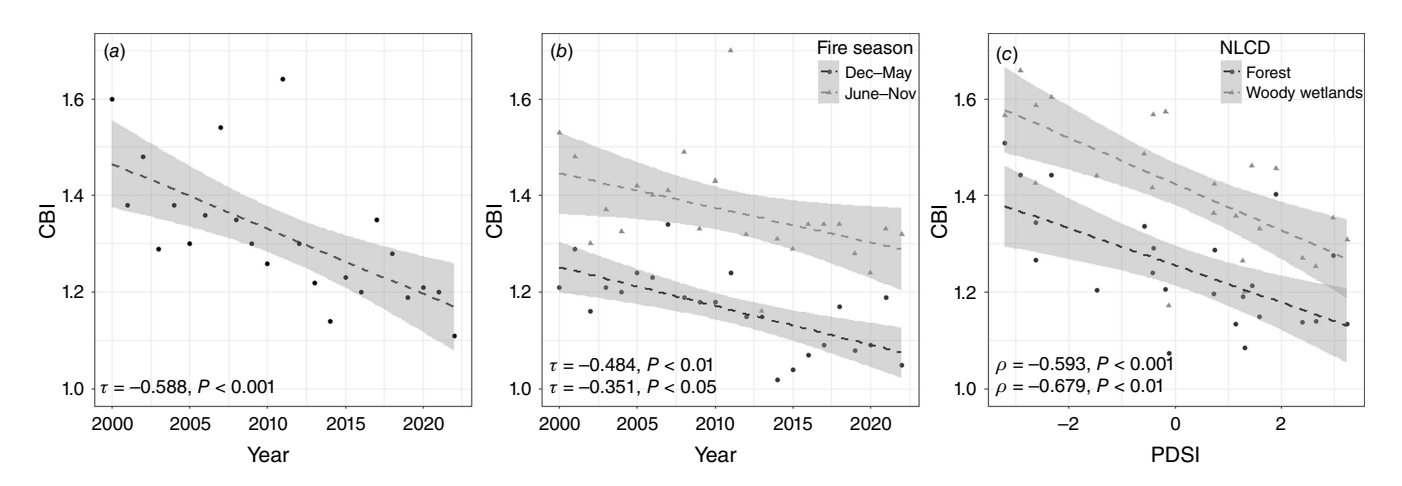


Fig. 8. Patterns in forest burn severity including (a) temporal trend in annual Composite Burn Index (CBI), (b) temporal trend within the season (December–May) dominated by prescribed fire compared with the season (June–November) dominated by wildfire, and (c) the correlation between the Palmer Drought Severity Index (PDSI) and CBI. Shaded area represents the 95% confidence interval of CBI severity values. Temporal trend significance evaluated using Mann–Kendall test for trends (τ) (a, b) and correlation significance evaluated using Spearman Rank Order Correlation (ρ) (c).

(Waldrop et al. 2012), the finding helps increase our confidence in the burn severity dataset. In addition, our result that woody wetlands showed a higher average burn severity compared with non-wetland evergreen forests was consistent with Malone et al. (2011), attributable in part to the dominance of highly flammable evergreen shrubs in the understorey of most forested wetlands in the region (Sackett 1975; Behm et al. 2004) as well as the accumulation of organic soils that can burn with high severity (Mickler et al. 2017). The high flammability and rapid regrowth of wetland understorey woody plants also likely contributed to the bald cypress/water tupelo forest type showing relatively high severity regardless of fire type and a small increase in severity in response to increasing fire frequency (Steel et al. 2015). Longleaf pine, in contrast, showed the greatest convergence of burn severity between prescribed and wildfires as fire frequency increased, attributable to the ecosystem's grass and pine needle litterdominated fuels and mineral soils that burn with relatively low intensity over a wide range of environmental conditions (Burns 1983; Reid et al. 2012; Mitchell et al. 2014). Loblolly pine and slash pine, the primary commercial tree species in the region, similarly showed comparable burn severity between prescribed and wildfires as fire frequency increased, underscoring the importance of periodic prescribed burning for protecting timber resources (Kobziar et al. 2015; Mason and Lashley 2021).

A declining trend in burn severity was observed within both wildfire and prescribed fire seasons. The finding was somewhat surprising given continental predictions of increasing wildfire hazard associated with climate change (Gao et al. 2021). However, regional climate projections and their implications for prescribed fire and wildfire are especially complex, with competing influences of higher

temperature, higher precipitation and more frequent droughts and hurricanes (Mitchell et al. 2014; Kupfer et al. 2020). The observed trend may instead be related to more recent patterns of drought and deluge, with extended regional droughts in the first decade of the 21st century (Pederson et al. 2012) and recent years (e.g. 2018–2022) seeing wetter conditions than average (Abatzoglou et al. 2018). Also, given that most fire in the region is prescribed, these patterns may reflect decisions by prescribed fire practitioners that compensate or override climatic patterns, as shown by Nowell et al. (2018). Regardless, improved algorithms for mapping trends in burn severity will prove essential in validating or challenging predicted regional trends of burn severity in the context of global climate change.

Exploring model performance

Previous endeavours to model burn severity have developed flexible frameworks (Parks et al. 2019; Picotte et al. 2020), but the models have struggled across the Southeast (Table 2). Similarly, although our model's RMSE and MSE were similar between the CONUS and the Southeast data, its explanatory power within the Southeast was substantially weaker, suggesting that predictive strength in the Southeast may be lower than has been achieved for the western US. One possible reason could be that prescribed fires in the Southeast often occur during leaf-off (dormant season) periods and target consumption of understorey vegetation. Lower pre-fire amounts of photosynthetic vegetation may influence CBI measurements and pre- to post-fire changes in spectral reflectance (Key and Benson 2006; Gallagher et al. 2020). However, we actually found that the Southeast had lower mean absolute residuals in the dormant season relative to the growing season, and further, that the Southeast's low and moderate burn severity plots showed lower mean absolute residuals relative to outside the Southeast. This demonstrated that our approach was not impacted by fire timing. Lower residuals from dormant season burns may reflect the more static condition of the post-burn environment prior to spring green-up, whereas initiation of vegetation recovery during the growing season is almost immediate.

Alternatively, the lower explanatory power of our model in the Southeast may instead be attributable to the minimal number of Southeast high-severity CBI plots (Gelman and Hill 2007). High-severity points represented <5% of the Southeast's CBI plots (Fig. 3) and showed higher mean absolute residuals relative to the non-Southeast (Table 3). The inclusion of climate normals (i.e. PET and PR) improved the CONUS-wide model performance in part by accounting for regional differences in climate-fire regime feedbacks (e.g. Wasserman and Mueller 2023). However, their inclusion could also have caused an under-prediction or negative bias of the region's minority case (Maxwell et al. 2018). Despite this source of uncertainty, utilising CONUS-wide CBI plot data allowed us to compensate for the lower availability of CBI plot data in the Southeast, in particular highseverity CBI plots, and enabled us to produce a scalable burn severity model that can potentially be applied outside of the region. Our modelling efforts can be used as a foundation for other global fire-prone regions that face similar challenges in characterising burn severity, but the transferability will depend on how similar the fire regimes and vegetation are to that represented by the CBI datasets.

Conclusion

Our scalable CBI model provides novel burn severity data that are more inclusive of the many small and prescribed fires across the Southeast compared with prior efforts. The consistency between expected and observed burn severity patterns suggests that our burn severity data can be successfully used for ecological and modelling applications. Trends and patterns in burn severity between vegetation and by fire types (e.g. prescribed versus wildfire) and fire frequency have important implications for prioritising local land management actions, such as hazardous fuel reduction and prescribed fire to manage wildfire risk (Kolden 2019), optimise forestry practices and monitor fire-dependent habitat condition (Alba et al. 2015). This improved capacity to predict burn severity in response to prescribed fire regimes, natural community types and forestry practices will contribute to improved estimates of atmospheric emissions (Jaffe et al. 2020; Kramer et al. 2023), residual carbon storage (Larkin et al. 2014), impacts on natural resources and accomplishment of ecological goals (Weiss et al. 2019). Future addition of high-severity CBI data within the Southeast and incorporation of more frequent imagery from compatible moderateresolution satellite missions, like the HLS dataset, will

further improve our capacity to map burn severity in the region.

Supplementary material

Supplementary material is available online.

References

Abatzoglou JT (2013) Development of gridded surface meteorological data for ecological applications and modelling. *International Journal of Climatology* **33**(1), 121–131. doi:10.1002/joc.3413

Abatzoglou JT, Dobrowski SZ, Parks SA, Hegewisch KC (2018) TerraClimate, a high-resolution global dataset of monthly climate and climatic water balance from 1958–2015. *Scientific Data* 5(1), 170191. doi:10.1038/sdata.2017.191

Addington RN, Hudson SJ, Hiers JK, Hurteau MD, Hutcherson TF, Matusick G, Parker JM (2015) Relationships among wildfire, prescribed fire, and drought in a fire-prone landscape in the southeastern United States. *International Journal of Wildland Fire* **24**(6), 778–783. doi:10.1071/WF14187

Alba C, Skálová H, McGregor KF, D'Antonio C, Pyšek P (2015) Native and exotic plant species respond differently to wildfire and prescribed fire as revealed by meta-analysis. *Journal of Vegetation Science* **26**(1), 102–113. doi:10.1111/jvs.12212

Alonso-González E, Fernández-García V (2021) MOSEV: a global burn severity database from MODIS (2000–2020). *Earth System Science Data* **13**, 1925–1938. doi:10.5194/essd-13-1925-2021

Barnett JP (1999) Longleaf pine ecosystem restoration: the role of fire. Journal of Sustainable Forestry 9(1–2), 89–96. doi:10.1300/ J091v09n01 07

Behm AL, Duryea ML, Long AJ, Zipperer WC (2004) Flammability of native understory species in pine flatwood and hardwood hammock ecosystems and implications for the wildland-urban interface. *International Journal of Wildland Fire* 13, 355–365. doi:10.1071/WF03075

Bigelow SW, Stambaugh MC, O'Brien JJ, Larson AJ, Battaglia MA (2017) Longleaf pine restoration in context: comparisons of frequent fire forests. In 'Ecological restoration and management of longleaf pine forests'. (Eds LK Kirkman, SB Jack) pp. 311–338. (CRC Press, Taylor & Francis Group)

Boisramé GFS, Brown TJ, Bachelet DM (2022) Trends in western USA fire fuels using historical data and modeling. *Fire Ecology* **18**, 8. doi:10.1186/s42408-022-00129-4

Bowman DMJS, Balch JK, Artaxo P, Bond WJ, Carlson JM, Cochrane MA, D'antonio CM, DeFries RS, Doyle JC, Harrison SP, Johnston FH, Keeley JE, Krawchuk MA, Kull CA, Marston JB, Moritz MA, Prentice IC, Roos CI, Scott AC, Swetnam TW, van der Werf GR, Pyne SJ (2009) Fire in the earth system. *Science* **324**(5926), 481–484. doi:10.1126/science.1163886

Burns RM (1983) (Technical compiler) Silvicultural systems for the major forest types of the United States. Agricultural Handbook 445. 191 p. (US Department of Agriculture, Forest Service: Washington, DC)

Busby S, Evers C, Holz A (2023) Patterns, drivers, and implications of postfire delayed tree mortality in temperate conifer forests of the western United States. *Ecosphere* **15**(4), e4805. doi:10.1002/ecs2.4805

Chen T, Guestrin C (2016) XGBoost: A scalable tree boosting system. In 'Proceedings of the 22nd ACM SIGKDD international conference on knowledge discovery and data mining'. (Eds B Krishnapuram, M Shah) pp. 785–794. (Association for Computing Machinery: New York, NY, USA)

Chuvieco E, Martín MP, Palacios A (2002) Assessment of different spectral indices in the red-near-infrared spectral domain for burned land discrimination. *International Journal of Remote Sensing* **23**(23), 5103–5110. doi:10.1080/01431160210153129

Cummins K, Noble J, Varner JM, Robertson KM, Hiers JK, Nowell HK, Simonson E (2023) The southeastern US prescribed fire permit

- database: hot spots and hot moments in prescribed fire across the southeastern USA. Fire 6(10), 372. doi:10.3390/fire6100372
- Donovan VM, Crandall R, Fill J, Wonkka CL (2023) Increasing large wildfire in the eastern United States. *Geophysical Research Letters* **50**(24), e2023GL107051. doi:10.1029/2023GL107051
- Dormann CF, Elith J, Bacher S, Buchmann C, Carl G, Carré G, Marquéz JRG, Gruber B, Lafourcade B, Leitão PJ, Münkemüller T, McClean C, Osborne PE, Reineking B, Schröder B, Skidmore AK, Zurell D, Lautenbach S (2013) Collinearity: a review of methods to deal with it and a simulation study evaluating their performance. *Ecography* **36**(1), 27–46. doi:10.1111/j.1600-0587.2012.07348.x
- Eidenshink JC, Schwind B, Brewer K, Zhu ZL, Quayle B, Howard SM (2007) A project for monitoring trends in burn severity. *Fire Ecology* **3**(1), 3–21. doi:10.4996/fireecology.0301003
- Epting J, Verbyla D, Sorbel B (2005) Evaluation of remotely sensed indices for assessing burn severity in interior Alaska using Landsat TM and ETM+. *Remote Sensing of Environment* **96**(3-4), 328–339. doi:10.1016/j.rse.2005.03.002
- Fowler C, Konopik E (2007) The history of fire in the southern United States. *Human Ecology Review* 14, 165–176.
- Franklin J, Serra-Diaz JM, Syphard AD, Regan HM (2016) Global change and terrestrial plant community dynamics. *Proceedings of the National Academy of Sciences* **113**(14), 3725–3734. doi:10.1073/pnas.1519911113
- Gallagher MR, Skowronski NS, Lathrop RG, McWilliams T, Green EJ (2020) An improved approach for selecting and validating burn severity indices in forested landscapes. *Canadian Journal of Remote Sensing* **46**(1), 100–111. doi:10.1080/07038992.2020.1735931
- Gao BC (1996) NDWI—A normalized difference water index for remote sensing of vegetation liquid water from space. *Remote Sensing of Environment* **58**(3), 257–266. doi:10.1016/S0034-4257(96)00067-3
- Gao P, Terando AJ, Kupfer JA, Morgan Varner J, Stambaugh MC, Lei TL, Kevin Hiers J (2021) Robust projections of future fire probability for the conterminous United States. *Science of The Total Environment* **789**, 147872. doi:10.1016/j.scitotenv.2021.147872
- García MJL, Caselles V (1991) Mapping burns and natural reforestation using Thematic Mapper data. *Geocarto International* **6**(1), 31–37. doi:10.1080/10106049109354290
- Gelman, A, Hill J (2007) 'Data analysis using regression and multilevel/hierarchical models.' (Cambridge University Press: Cambridge, UK)
- Godwin DR, Kobziar LN (2011) Comparison of burn severities of consecutive large-scale fires in Florida sand pine scrub using satellite imagery analysis. *Fire Ecology* **7**(2), 99–113. doi:10.4996/fireecology.0702099
- Hawbaker TJ, Vanderhoof MK, Schmidt GL, Beal YJ, Picotte JJ, Takacs JD, Falgout JT, Dwyer JL (2020a) The Landsat Burned Area algorithm and products for the conterminous United States. *Remote Sensing of the Environment* **244**, 111801. doi:10.1016/j.rse.2020. 111801
- Hawbaker TJ, Vanderhoof MK, Schmidt GL, Beal YJG, Picotte JJ, Takacs JD, Falgout JT, Dwyer JL (2020b) The Landsat Burned Area products for the conterminous United States (ver. 3.0, March 2022). US Geological Survey data release. doi:10.5066/P9QKHKTQ
- He K, Shen X, Anagnostou EN (2024) A global forest burn severity dataset from Landsat imagery (2003-2016). *Earth System Science Data* **16**(6), 3061–3081. doi:10.5194/essd-16-3061-2024
- Holden ZA, Smith AMS, Morgan P, Rollins MG, Gessler PE (2005) Evaluation of novel thermally enhanced spectral indices for mapping fire perimeters and comparisons with fire atlas data. *International Journal of Remote Sensing* **26**(21), 4801–4808. doi:10.1080/01431160500239008
- Homer CG, Dewitz JA, Jin S, Xian G, Costello C, Danielson P, Gass L, Funk M, Wickham J, Stehman S, Auch RF, Riitters KH (2020) Conterminous United States land cover change patterns 2001–2016 from the 2016 National Land Cover Database. *ISPRS Journal of Photogrammetry and Remote Sensing* **162**, 184–199. doi:10.1016/j.isprsjprs.2020.02.019
- Howard JL, Liang S (2019) US timber production, trade, consumption, and price statistics, 1965–2017. FPL-RP-701. (Research Paper-Forest Products Laboratory, USDA Forest Service)
- Howe AA, Parks SA, Harvey BJ, Saberi SJ, Lutz JA, Yocom LL (2022) Comparing Sentinel-2 and Landsat 8 for burn severity mapping in

- western North America. Remote Sensing 14(20), 5249. doi:10.3390/rs14205249
- Hudak AT, Morgan P, Bobbitt MJ, Smith AMS, Lewis SA, Lentile LB, Robichaud PR, Clark JT, McKinley RA (2007) The relationship of multispectral satellite imagery to immediate fire effects. *Fire Ecology* 3(1), 64–90. doi:10.4996/fireecology.0301064
- Huete A (1988) A soil-adjusted vegetation index (SAVI). Remote Sensing of Environment 25(3), 295–309. doi:10.1016/0034-4257(88)90106-X
- Huete A, Didan K, Miura T, Rodriguez EP, Gao X, Ferreira LG (2002) Overview of the radiometric and biophysical performance of the MODIS vegetation indices. *Remote Sensing of Environment* **83**, 195–213. doi:10.1016/S0034-4257(02)00096-2
- Huettermann S, Jones S, Soto-Berelov M, Hislop S (2023) Using Landsat time series and bi-temporal GEDI to compare spectral and structural vegetation responses after fire. *International Journal of Applied Earth Observation and Geoinformation* 122, 103403. doi:10.1016/j.jag. 2023.103403
- Hultquist C, Chen G, Zhao K (2014) A comparison of Gaussian process regression, random forests and support vector regression for burn severity assessment in diseased forests. *Remote Sensing Letters* **5**(8), 723–732. doi:10.1080/2150704X.2014.963733
- Humber ML, Boschetti L, Giglio L, Justice CO (2018) Spatial and temporal intercomparison of four global burned area products. *International Journal of Digital Earth* **12**(4), 460–484. doi:10.1080/17538947.2018.1433727
- Hunter ME, Robles MD (2020) Tamm review: the effects of prescribed fire on wildfire regimes and impacts: a framework for comparison. *Forest Ecology and Management* **475**, 118435. doi:10.1016/j.foreco. 2020.118435
- Jaffe DA, O'Neill SM, Larkin NK, Holder AL, Peterson DL, Halofsky JE, Rappold AG (2020) Wildfire and prescribed burning impacts on air quality in the United States. *Journal of the Air & Waste Management Association* **70**(6), 583–615. doi:10.1080/10962247.2020.1749731
- Johnson AS, Hale PE (2002) The historical foundations of prescribed burning for wildlife: a southeastern perspective. In 'Proceedings: The Role of Fire for Nongame Wildlife Management and Community Restoration: Traditional Uses and New Directions'. (Eds WM Ford, KR Russell, CE Moorman) General Technical Report NE-288. pp. 11–23. (USDA Forest Service, Northeastern Research Station: Newtown Square, PA)
- Keeley JE (2009) Fire intensity, fire severity and burn severity: a brief review and suggested usage. *International Journal of Wildland Fire* **18**(1), 116–126. doi:10.1071/WF07049
- Key CH, Benson NC (2006) Landscape assessment (LA): sampling and assessment methods. General Technical Report RMRS-GTR-164-CD.
 (USDA Forest Service, Rocky Mountain Research Station: Fort Collins, CO)
- Kobziar LN, Godwin D, Taylor L, Watts AC (2015) Perspectives on trends, effectiveness, and impediments to prescribed burning in the southern US *Forests* **6**(3), 561–580. doi:10.3390/f6030561
- Kolden CA (2019) We're not doing enough prescribed fire in the western United States to mitigate wildfire risk. *Fire* **2**, 30. doi:10.3390/fire2020030
- Kramer SJ, Huang S, McClure CD, Chaveste MR, Lurmann F (2023) Projected smoke impacts from increased prescribed fire activity in California's high wildfire risk landscape. *Atmospheric Environment* **311**, 119993. doi:10.1016/j.atmosenv.2023.119993
- Kupfer JA, Terando AJ, Gao P, Teske C, Hiers JK (2020) Climate change projected to reduce prescribed burning opportunities in the southeastern United States. *International Journal of Wildland Fire* 29(9), 764–778. doi:10.1071/WF19198
- LANDFIRE (2022) LANDFIRE public events geodatabase. Available at https://www.landfire.gov/reference/publicevents [last accessed 15 May 2024]
- Larkin NK, Raffuse SM, Strand TM (2014) Wildland fire emissions, carbon, and climate: US emissions inventories. *Forest Ecology and Management* **317**, 61–69. doi:10.1016/j.foreco.2013.09.012
- Liu Z, Wimberly MC (2015) Climatic and landscape influences on fire regimes from 1984 to 2010 in the western United States. *PLoS One* **10**(10), e0140839. doi:10.1371/journal.pone.0140839
- Lutz JA, Key CH, Kolden CA, Kane JT, Van Wagtendonk JW (2011) Fire frequency, area burned, and severity: a quantitative approach to

- defining a normal fire year. Fire Ecology 7, 51-65. doi:10.4996/fireecology.0702051
- Malone SL, Kobziar LN, Staudhammer CL, Abd-Elrahman A (2011) Modeling relationships among 217 fires using remote sensing of burn severity in southern pine forests. *Remote Sensing* 3(9), 2005–2028. doi:10.3390/rs3092005
- Mason DS, Lashley MA (2021) Spatial scale in prescribed fire regimes: an understudied aspect in conservation with examples from the southeastern United States. *Fire Ecology* **17**(3), 3. doi:10.1186/s42408-020-00087-9
- Maxwell AE, Warner TA, Fang F (2018) Implementation of machine-learning classification in remote sensing: an applied review. *International Journal of Remote Sensing* **39**(9), 2784–2817. doi:10.1080/01431161.2018.1433343
- Melvin MA (2020) National prescribed fire use survey report. Technical Bulletin 04-20. 9 p. (Coalition of Prescribed Fire Councils, Inc. and National Association of State Foresters)
- Meng R, Zhao F (2017) Remote sensing of fire effects: a review for recent advances in burned area and burn severity mapping. In 'Remote sensing of hydrometeorological hazards'. (Eds GP Petropoulos, T Islam) pp. 261–276. (CRC Press: Boca Raton, FL, USA)
- Menick C, Vanderhoof MK, Picotte J, Hawbaker TJ (2024) Annual burn severity mosaics for the southeastern United States (2000-2022). US Geological Survey data release. doi:10.5066/P1497B4P
- Mickler RA, Welch DP, Bailey AD (2017) Carbon emissions during wildland fire on a North American temperate peatland. *Fire Ecology* **13**, 34–57.
- Miller CW, Harvey BJ, Kane VR, Moskal LM, Alvarado E (2023) Different approaches make comparing studies of burn severity challenging: a review of methods used to link remotely sensed data with the Composite Burn Index. *International Journal of Wildland Fire* **32**(4), 449–475. doi:10.1071/WF22050
- Miller JD, Thode AE (2007) Quantifying burn severity in a heterogeneous landscape with a relative version of the delta Normalized Burn Ratio (dNBR). *Remote Sensing of Environment* **109**(1), 66–80. doi:10.1016/j.rse.2006.12.006
- Miller JD, Knapp EE, Key CH, Skinner CN, Isbell CJ, Creasy RM, Sherlock JW (2009) Calibration and validation of the relative differenced Normalized Burn Ratio (RdNBR) to three measures of fire severity in the Sierra Nevada and Klamath Mountains, California, USA. *Remote Sensing of Environment* 113, 645–656. doi:10.1016/j.rse.2008.11.009
- Mitchell RJ, Liu Y, O'Brien JJ, Elliott KJ, Starr G, Miniat CF, Hiers JK (2014) Future climate and fire interactions in the southeastern region of the United States. *Forest Ecology and Management* **327**, 316–326. doi:10.1016/j.foreco.2013.12.003
- Murphy MA, Evans JS, Storfer A (2010) Quantifying *Bufo boreas* connectivity in Yellowstone National Park with landscape genetics. *Ecology* **91**, 252–261. doi:10.1890/08-0879.1
- Noss RF, Platt WJ, Sorrie BA, Weakley AS, Means DB, Costanza J, Peet RK (2015) How global biodiversity hotspots may go unrecognized: lessons from the North American coastal plain. *Diversity and Distributions* **21**(2), 236–244. doi:10.1111/ddi.12278
- Nowell HK, Holmes CD, Robertson K, Teske C, Hiers JK (2018) A new picture of fire extent, variability, and drought interaction in prescribed fire landscapes: insights from Florida Government records. *Geophysical Research Letters* **45**, 7874–7884. doi:10.1029/2018GL078679
- Omernik JM, Griffith GE (2014) Ecoregions of the conterminous United States: evolution of a hierarchical spatial framework. *Environmental Management* **54**(6), 1249–1266. doi:10.1007/s00267-014-0364-1
- Parks S, Abatzoglou JT (2020) Warmer and drier fire seasons contribute to increases in area burned at high severity in western US forests from 1985 to 2017. *Geophysical Research Letters* **47**(22), e2020GL089858. doi:10.1029/2020GL089858
- Parks SA, Dillon GK, Miller C (2014) A new metric for quantifying burn severity: the Relativized Burn Ratio. *Remote Sensing* **6**(3), 1827–1844. doi:10.3390/rs6031827
- Parks SA, Holsinger LM, Koontz MJ, Collins L, Whitman E, Parisien MA, Loehman RA, Barnes JL, Bourdon JF, Boucher J, Boucher Y, Caprio AC, Collingwood A, Hall RJ, Park J, Saperstein LB, Smetanka C, Smith RJ, Soverel N (2019) Giving ecological meaning to satellite-derived fire severity metrics across North American forests. *Remote Sensing* 11(14), 1735. doi:10.3390/rs11141735

- Pederson N, Bell A, Knight TA, Leland C, Malcomb N, Anchukaitis KJ, Tackett K, Scheff J, Brice A, Catron B (2012) A long-term perspective on a modern drought in the American Southeast. *Environmental Research Letters* 7(1), 014034. doi:10.1088/1748-9326/7/1/014034
- Picotte JJ, Robertson K (2011a) Timing constraints on remote sensing of wildland fire burned area in the southeastern US. *Remote Sensing* 3(8), 1680–1690. doi:10.3390/rs3081680
- Picotte JJ, Robertson KM (2011b) Validation of remote sensing of burn severity in south-eastern US ecosystems. *International Journal of Wildland Fire* **20**(3), 453–464. doi:10.1071/WF10013
- Picotte J, Arkle RS, Bastian H, Benson N, Cansler A, Caprio T, Dillon G, Key C, Klein RN, Kolden CA, Kopper K, Lutz JA, Meddens AJH, Ohlen D, Parks SA, Peterson DW, Pilliod D, Prichard S, Robertson K, Sparks A, Thode A (2019) Composite Burn Index (CBI) data for the conterminous US, collected between 1996 and 2018. US Geological Survey data release. doi:10.5066/P91BH1BZ
- Picotte JJ, Bhattarai K, Howard D, Lecker J, Epting J, Quayle B, Benson N, Nelson K (2020) Changes to the Monitoring Trends in Burn Severity program mapping production procedures and data products. *Fire Ecology* **16**(1), 16. doi:10.1186/s42408-020-00076-y
- Picotte JJ, Cansler CA, Kolden CA, Lutz JA, Key C, Benson NC, Robertson KM (2021) Determination of burn severity models ranging from regional to national scales for the conterminous United States. *Remote Sensing of Environment* **263**, 112569. doi:10.1016/j.rse.2021. 112569
- Pinty B, Verstraete MM (1992) GEMI: a non-linear index to monitor global vegetation from satellites. *Vegetatio* **101**, 15–20. doi:10.1007/BF00031911
- Radeloff VC, Mockrin MH, Helmers D, Carlson A, Hawbaker TJ, Martinuzzi S, Schug F, Alexandre PM, Kramer HA, Pidgeon AM (2023) Rising wildfire risk to houses in the United States, especially in grasslands and shrublands. *Science* 382, 702–707. doi:10.1126/ science.ade9223
- Randerson JT, van der Werf GR, Giglio L, Collatz GJ, Kasibhatla PS (2017) 'Global fire emissions database; Version 4.1 (GFEDv4).' (ORNL DAAC: Oak Ridge, TN, USA)
- Reid AM, Robertson KM, Hmielowski TL (2012) Predicting litter and live herb fuel consumption during prescribed fires in native and old-field upland pine communities of the southeastern United States. *Canadian Journal of Forest Research* **42**, 1611–1622.
- Reiner AL, Baker CR, Wahlberg MM (2022) 'Geospatial data for 2017-2018 wildland fires in the southwestern United States used for region-specific Rapid Assessment of Vegetation Condition after Wildfire (RAVG) models: burned area boundaries and burn indices derived from Landsat and Sentinel-2 satellite imagery.' (Forest Service Research Data Archive: Fort Collins, CO) doi:10.2737/RDS-2022-0019
- Ruefenacht B, Finco MV, Nelson MD, Czaplewski R, Helmer EH, Blackard JA, Holden GR, Lister AJ, Salajanu D, Weyermann D, Winterberger K (2008) Conterminous US and Alaska forest type mapping using forest inventory and analysis data. *Photogrammetric Engineering & Remote Sensing* **74**(11), 1379–1388. doi:10.14358/PERS.74.11.1379
- Ryan KC, Knapp EE, Varner JM (2013) Prescribed fire in North American forests and woodlands: history, current practice, and challenges. *Frontiers in Ecology and the Environment* **11**, 15–24. doi:10.1890/120329
- Saberi SJ, Harvey BJ (2023) What is the color when black is burned? Quantifying (re)burn severity using field and satellite remote sensing indices. *Fire Ecology* **19**(1), 24. doi:10.1186/s42408-023-00178-3
- Sackett SS (1975) Scheduling prescribed burns for hazard reduction in the Southeast. *Journal of Forestry* **73**, 143–147.
- Salvia M, Ceballos DC, Grings F, Karszenbaum H, Kandus P (2012) Postfire effects in wetland environments: landscape assessment of plant coverage and soil recovery in the Paraná River Delta marshes, Argentina. Fire Ecology 8, 17–37. doi:10.4996/fireecology.0802017
- Sherrouse BC, Hawbaker TJ (2023) HOPS: Hyperparameter optimization and predictor selection v1.0, US Geological Survey Software Release. doi:10.5066/P9P81HUR.
- Short KC (2022) 'Spatial wildfire occurrence data for the United States, 1992–2020 [FPA_FOD_20221014]', 6th edn. (Forest Service Research Data Archive: Fort Collins, CO) doi:10.2737/RDS-2013-0009.6 [accessed 20 October 2023]
- Slocum MG, Platt WJ, Beckage B, Panko B, Lushine JB (2007) Decoupling natural and anthropogenic fire regimes: a case study in

- Everglades National Park, Florida. *Natural Areas Journal* **27**(1), 41–55. doi:10.3375/0885-8608(2007)27[41:DNAAFR]2.0.CO;2
- Smith AMS, Drake NA, Wooster MJ, Hudak AT, Holden ZA, Gibbons CJ (2007) Production of Landsat ETM+ reference imagery of burned areas within Southern African savannahs: comparison of methods and application to MODIS. *International Journal of Remote Sensing* **28**(12), 2753–2775. doi:10.1080/01431160600954704
- Steel ZL, Safford HD, Viers JH (2015) The fire frequency-severity relationship and the legacy of fire suppression in California forests. *Ecosphere* **6**(1), 1–23. doi:10.1890/ES14-00224.1
- Tall Timbers (2024) SE FireMap. Available at https://www.landscapepartnership.org/networks/working-lands-for-wildlife/wild-land-fire/fire-mapping/regional-fire-mapping/se-firemap [accessed 22 November 2024]
- Teske C, Vanderhoof MK, Hawbaker TJ, Noble J, Hiers JK (2021) Using the Landsat burned area products to derive fire history relevant for fire management and conservation in the state of Florida, southeastern USA. *Fire* **4**, 26. doi:10.3390/fire4020026
- Thomas DS, Butry DT (2014) Areas of the US wildland–urban interface threatened by wildfire during the 2001–2010 decade. *Natural Hazards* **71**, 1561–1585. doi:10.1007/s11069-013-0965-7
- Trigg S, Flasse S (2001) An evaluation of different bi-spectral spaces for discriminating burned shrub-savannah. *International Journal of Remote Sensing* **22**(13), 2641–2647. doi:10.1080/01431160110053185
- Tucker CJ (1979) Red and photographic infrared linear combinations for monitoring vegetation. *Remote Sensing of Environment* **8**(2), 127–150. doi:10.1016/0034-4257(79)90013-0
- US Geological Survey (USGS) (2022) Protected Areas Database of the United States (PAD-US) 3.0, Gap Analysis Project (GAP), US Geological Survey data release. doi:10.5066/P9O9LO4B
- Vanderhoof MK, Hawbaker JJ, Teske C, Ku A, Noble J, Picotte J (2021) Mapping wetland burned area from Sentinel-2 across the southeastern United States and its contributions relative to Landsat-8 (2016-2019). Fire 4(3), 52. doi:10.3390/fire4030052

- Vanderhoof MK, Hawbaker TJ, Teske C, Noble J, Smith J (2022) Contemporary (1984-2020) fire history metrics for the conterminous United States and ecoregional differences by land ownership. *International Journal of Wildland Fire* **31**(12), 1167–1183. doi:10.1071/WF22044
- van der Werf GR, Randerson JT, Giglio L, van Leeuwen TT, Chen Y, Rogers BM, Mu M, van Marle MJE, Morton DC, Collatz GJ, Yokelson RJ, Kasibhatla PS (2017) Global fire emissions estimates during 1997–2016. *Earth System Science Data* **9**, 697–720. doi:10.5194/essd-9-697-2017
- Waldrop TA, Goodrick SL, Harper CA, Towne EG (2012) 'Introduction to prescribed fire in Southern ecosystems'. Science Update SRS-054. (USDA Forest Service Southern Research Station: Asheville, NC)
- Wasserman TN, Mueller SE (2023) Climate influences on future fire severity: a synthesis of climate–fire interactions and impacts on fire regimes, high-severity fire, and forests in the western United States. *Fire Ecology* **19**, 43. doi:10.1186/s42408-023-00200-8
- Weiss SA, Toman EL, Corace III RG (2019) Aligning endangered species management with fire-dependent ecosystem restoration: manager perspectives on red-cockaded woodpecker and longleaf pine management actions. *Fire Ecology* **15**, 19. doi:10.1186/s42408-019-0026-z
- Whitman E, Parisien MA, Holsinger LM, Park J, Parks SA (2020) A method for creating a burn severity atlas: an example from Alberta, Canada. *International Journal of Wildland Fire* **29**(11), 995–1008. doi:10.1071/WF19177
- Zhu Z, Woodcock CE (2014) Automated cloud, cloud shadow, and snow detection in multitemporal Landsat data: an algorithm designed specifically for monitoring land cover change. *Remote Sensing of Environment* **152**, 217–234. doi:10.1016/j.rse.2014.06.012
- Zhu Z, Key CH, Benson NC (2006) Evaluate sensitivities of burn-severity mapping algorithms for different ecosystems and fire histories in the United States. pp. 1–36. (Final Report to the Joint Fire Science Program, US Department of Interior: Washington, DC)

Data availability. The annual (2000–2022) CBI burn severity data (30 m resolution) are available for download (Menick et al. 2024).

Conflicts of interest. The authors declare they have no conflicts of interest.

Declaration of funding. This research was funded by the US Department of Agriculture, Natural Resources Conservation Service ('SE FireMap, Phase 2 – Enhanced burned area products and decision support tools') and the US Geological Survey's National Land Imaging and Land Change Science Programs.

Acknowledgements. We appreciate support on graphics from Jeremy Havens, CBI data from Alicia Reiner and feedback on earlier versions from Roy Petrakis and the journal reviewers. Any use of trade, firm, or product names is for descriptive purposes only and does not imply endorsement by the US Government.

Author affiliations

^AUS Geological Survey, Geosciences and Environmental Change Science Center, Denver Federal Center, MS980, Denver, CO 80225, USA.

^BUS Geological Survey, Earth Resources Observation and Science (EROS) Center, 47914 52nd Street, Sioux Falls, SD 57198, USA.

^CTall Timbers Research Station, 13093 Henry Beadel Drive, Tallahassee, FL 32312, USA.